The Utility of Isotropic 3D Magnetic Resonance Imaging in Assessing Painful Total Ankle Replacements

Ji Lin, MD[1] , Carolyn M. Sofka, MD[1], Constantine A. Demetracopoulos, MD[2], and Hollis G. Potter, MD[1]

Keywords: total ankle arthroplasty, total ankle replacement, MRI, metal artifact reduction sequences, aseptic loosening, osteolysis, infection

Introduction

The use of total ankle replacement (TAR) in select patients with end-stage arthritis has increased over the past 10-15 years, largely due to improved implant designs and operative techniques. Survivorship for current-generation implants has also improved, although failure rates remain higher than those for hip or knee replacements.[29,30,43] The ability to identify early signs of failure can alter treatment algorithms, allowing interventions to potentially save the prothesis rather than necessitating revision or conversion to arthrodesis.[1,20]

Currently, radiography is the mainstay for TAR imaging for both routine follow-up and to assess postoperative patients who present with pain. Radiography is a useful tool to assess component alignment, changes in component positioning, periprosthetic lucency, and periprosthetic fracture. Computed tomography (CT) performs well to further characterize these findings, with metal artifact reduction techniques used to mitigate photon starvation and beam-hardening artifact that can obscure the bone-metal interface, thereby allowing better visualization of periprosthetic fractures and osteolysis. However, both radiography and CT are limited in evaluation of the periprosthetic soft tissue structures. Single-photon emission computed tomography combined with conventional computed tomography (SPECT-CT) partially circumvents the limitations of conventional CT by using functional bone scintigraphy to identify and localize areas of abnormal metabolic uptake. Despite bone scintigraphy being a sensitive modality for increased metabolic activity, there is physiologic uptake after TAR and the degree of this uptake over time is unknown.[19] Ultrasonography is occasionally used to detect periprosthetic soft tissue abnormalities and to guide aspiration when there is a concern for infection but cannot visualize the internal architecture of the osseous structures or the bone-metal interface.

Magnetic resonance imaging (MRI) is less commonly performed for evaluation of TAR but has great diagnostic potential given its ability to characterize both osseous and soft tissue abnormalities. MRI can also identify low-grade injuries such as periprosthetic stress reaction because of its ability to detect bone marrow edema, which cannot be seen with other imaging modalities. However, conventional fast spin-echo (FSE) MR techniques can be significantly limited by signal loss and encoding distortion because of magnetic field inhomogeneities generated by the metal components. The advent of 3-dimensional multispectral imaging (3D MSI) MR imaging techniques such as multi-acquisition variable resonance image combination selective (MAVRIC SL; GE Healthcare) mitigate the encoding distortions and artifacts, thus dramatically improving image quality and ease of image interpretation. The purpose of this case series

[1]Department of Radiology and Imaging, Hospital for Special Surgery, New York, NY, USA
[2]Department of Orthopedic Surgery, Foot and Ankle Service, Hospital for Special Surgery, New York, NY, USA

Corresponding Author:
Ji Lin, MD, Department of Radiology and Imaging, Hospital for Special Surgery, 535 E 70th Street, New York, NY 10021, USA.
Email: linji@hss.edu

is to outline techniques for optimization of MRI of the TAR, discuss common postoperative complications, and illustrate their MRI appearances.

MR Imaging Technique

Technical Considerations

MR imaging of the ankle arthroplasty requires optimized FSE pulse sequences and 3D MSI to adequately evaluate the tissues surrounding the implant. These sequences compensate for encoding distortions caused by differences in magnetic susceptibilities between the metallic implant components and the surrounding tissues. Magnetization induced in any given object, in proportion to its magnetic susceptibility and the strength of the external magnetic field, causes local magnetic field distortion.[12] Thus, the effect of field distortion on the image depends on the strength of the external magnetic field as well as the size, shape, and type of metal being imaged.[16] The intrinsic properties of the implant cannot be modified at the time of scanning, but use of a 1.5-tesla (T) rather than a 3-T field strength results in less pronounced field distortion.

Different metallic implant materials have different magnetic susceptibilities (χ) and, of the metals used in standard total ankle systems, χ of cobalt-chromium-molybdenum alloy is the largest, approximately 1300 parts-per-million (ppm); cobalt-chromium has a χ of 900 ppm; titanium a χ of 182 ppm; and tantalum a χ of 178 ppm.[28] Because of the χ of these materials, particularly the cobalt-chromium-molybdenum and cobalt-chromium alloys, large disturbances are generated in the magnetic field. These metal-induced inhomogeneities of the static magnetic field result in accelerated dephasing of local spins, yielding signal loss, as well as alteration of local spin precession frequencies, yielding signal misregistration to an incorrect location along the frequency-encoded in-plane and slice-select through-plane directions.[16] Displaced signal manifests on the resultant images as spatial distortion with areas of signal void and adjacent signal pile-up.

Fast spin-echo (FSE) pulse sequences mitigate accelerated spin dephasing from field inhomogeneity through 180° refocusing pulses and are therefore preferred over gradient echo sequences that amplify metal-induced signal loss. The degree of susceptibility artifact is also inversely proportional to the strength of the frequency-encoded in-plane and slice-select gradients. A wider receiver bandwidth and thinner slices yield an increase in the amplitude of the frequency-encoded gradients, thereby reducing the degree of in-plane and through-plane spatial misregistration.[15] Increasing the matrix size improves spatial resolution, allowing better definition at the implant-tissue interfaces. Although a wider receiver bandwidth and smaller voxel size does result in a decreased signal-to-noise ratio with a greater number of excitations required, the use of stronger gradients also results in shorter inter-echo spacing, allowing for longer echo trains and overall shorter scan times.[15,16]

Although optimized FSE metal artifact reduction sequences (MARS) can allow better assessment of tissue surrounding the metal implant, the residual through-plane distortion can still obscure tissue visualization close to the metal. Therefore, it is important to utilize MARS as well as 3D MSI techniques such as MAVRIC SL, which are now available across vendors.[27] MAVRIC SL acquisitions reduce magnetic susceptibility artifact by combining data sampled at multiple frequency offsets from the Larmor frequency to capture signal that would otherwise be misregistered.[45]

HyperMAVRIC SL (which enables isotropic MAVRIC SL acquisitions) is preferred over conventional MAVRIC SL.[23] In the HyperMAVRIC SL technique, a short spectral calibration scan is performed to determine the number of spectral bins required to provide frequency coverage that is broad enough to encompass the field distortion caused by the specific metallic composition of the implant to be scanned. This could potentially permit fewer spectral bins to be acquired, thereby decreasing scan time. This also results in improved image quality since unnecessary acquisition of spectral bins that contain little to no signal only contributes to noise and ghosting artifact.[45] The time savings from acquiring fewer spectral bins, as well as from an increased echo train length (ETL) with variable flip-angles, can then be applied to reducing slice thickness, allowing for an isotropic sequence that can be reformatted into other planes.[45]

The favored fat-suppression technique for prosthesis imaging is short TI (inversion time) inversion recovery (STIR), which provides more uniform fat suppression than chemical shift-selective (CHESS) fat saturation. Metal-induced field heterogeneity can shift the water and main fat frequency peaks such that the fat-saturation radiofrequency pulse used in the chemical shift-selective technique falls outside the fat frequency range, resulting in failure of fat saturation or inadvertent water suppression around the metal implant.[11] In contrast, the STIR technique, which is dependent on differences in T1 longitudinal recovery of different tissue types, is relatively insensitive to magnetic field heterogeneity and thus preferred for use around metal.

Additional considerations in the foot and ankle include the frequent concurrent presence of other orthopaedic hardware, which can be composed of stainless-steel alloys and generate a large amount of magnetic field inhomogeneity. Other procedures that may be performed at the time of TAR and require hardware include prophylactic fixation of the medial malleolus, calcaneal osteotomy, subtalar and/or talonavicular arthrodesis, and midfoot arthrodesis.

Table 1. Pulse Sequences.

Parameters	Axial FSE	Coronal FSE	Sagittal FSE	HyperMAVRIC SL Spectral Calibration[a]	Sagittal HyperMAVRIC SL[b]	Sagittal MAVRIC SL[c]
Acquisition type	2D FSE	2D FSE	2D FSE	3D FSE	3D FSE	3D FSE
Weighting	Intermediate	Intermediate	Intermediate	Intermediate	Intermediate	STIR
Repetition time (ms)	3500-6000	4000-5000	4000-5000	1460	3500	4000-5000
Echo time (ms)	23-32	21-31	27-35	8-8.3	8-10	8-10
Fat suppression	None	None	None	None	None	Inversion pulse at 150 ms
Echo train length	16-24	16-24	16-24	16	48	24
Receiver bandwidth (Hz/pixel)	488	488	488	488	488	488
Refocusing flip angle (degrees)	160	160	160	110	110	110
Field of view (mm)	200 × 200	200 × 200	200 × 200	240 × 240	240 × 240	240 × 240
Matrix	512 × 256	512 × 256	512 × 256	128 × 32	240 × 240	256 × 192
Slice thickness/gap (mm)	4/0	4/0	3/0	6/0	1/0	2.5-3.5/0
No. of signals acquired	2	2	2	0.5	0.5	0.5
No phase wrap factor	2	2	2	1	1	1
In-plane frequency encoding direction	Column (anterior to posterior)	Column (superior to inferior)	Row (anterior to posterior)	Variable[a]	Column (superior to inferior)	Column (superior to inferior)
Gadolinium-based contrast agent	None	None	None	None	None	None
Scan time (minutes)[d]	3-8	3-8	3-8	1	4-10	4-8

Abbreviations: FSE, fast spin-echo; 2D, 2-dimensional; 3D, 3-dimensional; MAVRIC SL, multi-acquisition variable resonance image combination selective; MRI, magnetic resonance imaging; ms, milliseconds; mm, millimeters; PACS, picture archiving and communication system; STIR, short TI (inversion time) inversion recovery.

[a]Plane of the spectral calibration scan is variable, as is the direction of in-plane frequency encoding.

[b]This isotropic HyperMAVRIC SL sequence acquired in the sagittal plane is used to create reformatted images in the coronal and axial planes, saved to our PACS by the MRI technologists. It can also be used to easily and quickly create reformations in any plane as desired at the PACS workstation.

[c]Our routine protocol includes only 1 sagittal fat-suppressed sequence. However, if there is any finding that requires clarification on the routine sequences, fat-suppressed images in one (usually axial) or more other planes are frequently also acquired.

[d]The approximate ranges of time are typical of the clinical application.

Along with the arthroplasty components, artifact from the hardware associated with these procedures can obscure much of the field of view if the appropriate techniques are not implemented.

In our institution, MR imaging of the TAR is performed on a 1.5-T clinical scanner (GE Discovery MR450 or Optima MR450w scanner; GE Healthcare) with an 8-channel foot and ankle coil (GE Healthcare). A suggested pulse sequence protocol is detailed in Table 1.

Practical Considerations

Nonweightbearing MR imaging is performed with the patient in the supine position, usually with the ankle in a close-to-neutral degree of flexion. Dedicated foot and ankle multichannel quadrature surface coils facilitate high spatial resolution imaging.[16,42] The MR images should include the entire ankle and hindfoot in anteroposterior and mediolateral directions and should extend from the level of the distal tibia above the ankle to cover the entirety of the plantar soft tissues inferiorly. The coronal sequence may be prescribed in the coronal plane to the foot or in the direct coronal plane to the ankle.

STIR MAVRIC SL images are helpful in the identification of stress reactions/fractures, periprosthetic osseous resorption, synovitis, joint effusion, and soft tissue edema and fluid collections.[15,16] The HyperMAVRIC SL sequence enables dramatically improved evaluation of the bone-metal interface as well as visualization of the anatomy in all desired planes. Intermediate-weighted FSE pulse sequences with high spatial resolution are important for assessing the soft tissues beyond the region immediately

surrounding the bone-metal interface because of their high signal-to-noise ratio, fluid sensitivity, and favorable contrast-to-noise ratio.[16]

T2-weighted sequences with echo times greater than 50 milliseconds have poor signal-to-noise ratios whereas T1-weighted sequences provide poor fluid-to-synovium contrast.[16] However, T1-weighted imaging with gadolinium contrast, although not routinely used in MR evaluation of the painful ankle replacement, is often helpful in the setting of infection to identify soft tissue abscesses and septic tenosynovitis. In these cases, we do not use inversion recovery fat suppression technique as gadolinium-enhanced tissues have a similar T1 relaxation time to fat. Instead, we obtain both pre- and postcontrast sequences without fat suppression, usually in the axial plane, as well as an additional postcontrast sequence in an orthogonal plane. A wide receiver bandwidth should be used to decrease metal artifact. Alternatively, 3D MSI techniques such as MAVRIC SL may also be obtained with T1-weighting.

MRI Appearance of Complications

Studies examining survivorship of TAR based on multiple national joint registries have found 10-year survivorships in the range of approximately 70% to 90%, with some dependence on surgeon experience.[5,6,21] The most common reason for implant failure requiring revision is aseptic loosening.[39] Other complications include periprosthetic fracture, stress reaction, subsidence, expansile osteolysis, polyethylene liner fracture/displacement, infection, gutter impingement, adjacent joint degeneration, and heterotopic ossification.

Aseptic Loosening—Osseous Resorption and Cystic Osteolysis

Aseptic loosening refers to loss of fixation at the bone-metal interface of the prosthesis, in the absence of infection, with approximately 40% of TAA revisions performed for this reason.[17,31,37,39] The causes of aseptic loosening are multifactorial and likely include micromotion at the bone-metal interface due to shear and rotational forces, localized tissue necrosis with development of a reparative membrane, and shedding of polyethylene particles inducing a cell-mediated reaction inhibiting bone ingrowth and the development of fluid or a fibrous interface between the implant and the bone.[2,3,7,22,26,37,44] When minimal, aseptic loosening will be asymptomatic and can be monitored clinically and radiologically for progression as imaging findings of aseptic loosening may precede clinical symptoms.[33] An accurate and reliable way to evaluate the bone-metal interface of the prosthesis is necessary for this purpose.

Depending on the material composition of the prosthesis, artifact often obscures the area of interest at the bone-metal interface on conventional FSE sequences. Therefore,

MRI with metal optimization techniques is essential (Figure 1). An intact bone-metal interface demonstrates direct contact of the implant with the surrounding bone (Figure 1C). Lack of osseous integration is reflected by separation of the implant component and the bone along their interface. A separation of 1 to 2 mm represents formation of a "fibrous membrane," akin to that seen in hip and knee arthroplasties, whereas a separation of greater than 2 mm in thickness may be qualified as osseous resorption.[15,16] When osseous resorption becomes essentially circumferential, there is a high likelihood that the component is loose (Figure 2).

Osseous resorption is often associated with more expansile regions of cystic osteolysis, likely a result of an immune-mediated macrophage response to, and phagocytosis of, particulate debris, with an upregulation of osteoclast activity and a downregulation of osteoblast activity.[38,40] Macrophages differentiate into osteoclasts and existing osteoclasts are activated, resulting in osteolysis.[4,14,38,40] Another theory, given that some periprosthetic cysts have been found to be without polyethylene debris histologically, attributes cyst formation to high intra-articular fluid pressure in a reactive joint decompressing through exposed subchondral bone that is not covered by the prosthesis.[14,33]

Enlarging cysts should be treated operatively to reduce the risk of implant failure. Treatment of expansile osteolysis includes operative curettage and bone grafting.[33] MRI is useful for identifying cystic osteolysis early, before the implant becomes loose, thus allowing an intervention to reestablish bone around the implant without the need for revision. Although cystic osteolysis extends further from the bone-metal interface than fibrous membrane, it may still be obscured by prominent metal artifact on conventional FSE sequences, so metal optimization techniques should always be used (Figure 3). MRI can also be used to characterize patterns of bone resorption/osteolysis as cavitary, segmental, and combined osteolytic defects, a classification system used by the American Academy of Orthopaedic Surgeons for hip and knee replacements.[17] In the setting of polyethylene wear-induced cystic osteolysis, an inflammatory polymeric synovitis may be present and is well demonstrated on MRI (Figure 4).

Subsidence

During the first months after TAR, slight migration and settling of the components may occur, but this should not progress after 6 months.[37] Subsidence is diagnosed if there is greater than 5 mm depression of the tibial or talar component and may be associated with greater than 5 degrees of angular deformity (Figure 3D).[37] Subsidence is a relatively common postoperative complication, with a rate of 10.7% as reported in a literature review by Glazebrook et al.[18] However, tibial component subsidence has become much
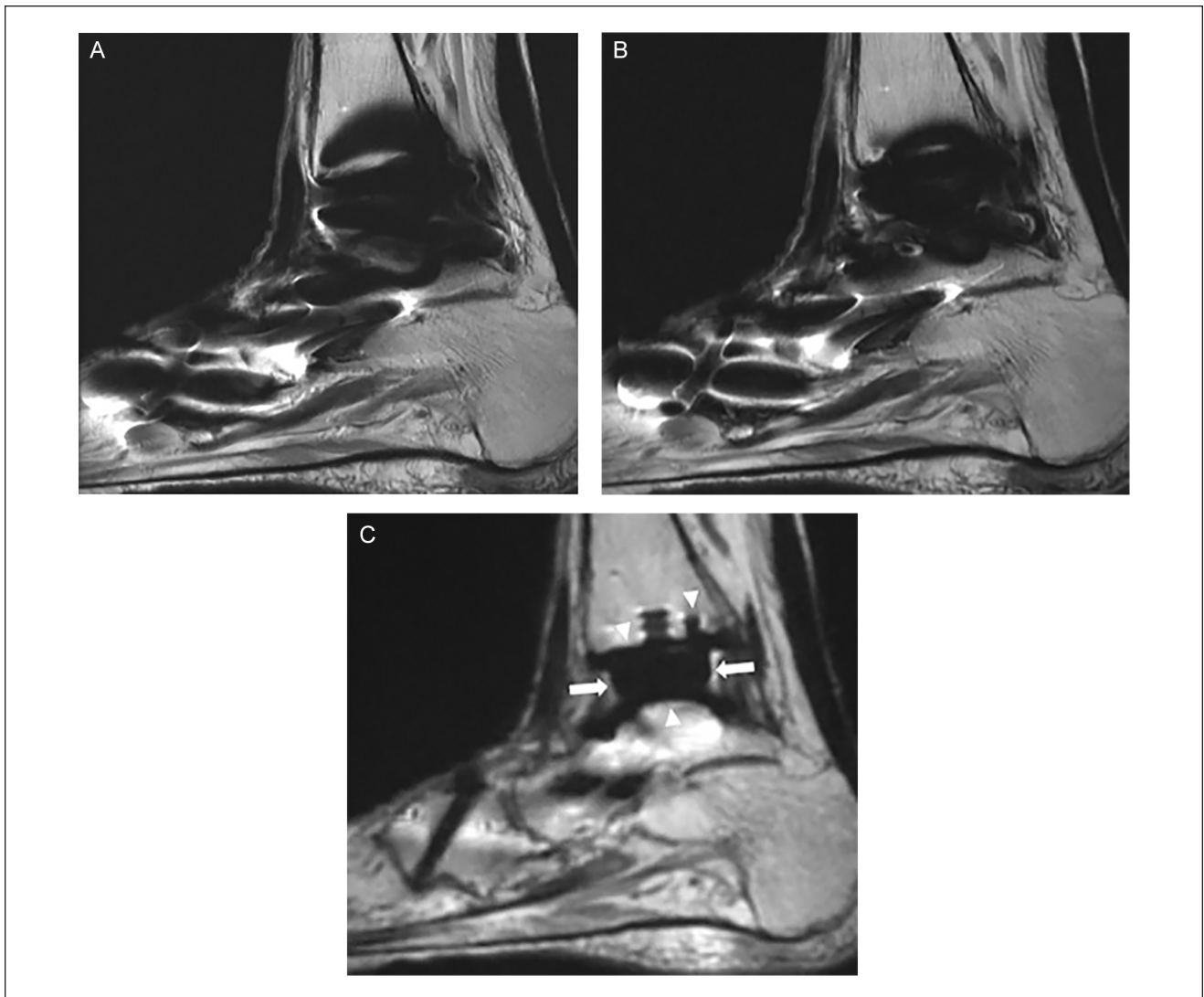
Figure 1. Vantage TAR in a 70-year-old woman who has also undergone talonavicular and Lapidus arthrodeses. (A) Sagittal images through the same plane demonstrate marked signal loss and displacement related to metal-induced field inhomogeneity, which completely obscures the periprosthetic tissues on the intermediate-weighted midbandwidth fast spin-echo (FSE) image, only slightly improved when performed with high receiver bandwidth (B). In contrast, (C) the isotropic HyperMAVRIC SL image has dramatically less artifact, allowing evaluation of the periprosthetic tissues and the polyethylene liner (arrows). The clearly visualized bone-metal interface (arrowheads) is intact, without abnormal separation.

less common since newer implant designs have improved initial tibial component fixation.[37] Similar to aseptic loosening, the cause of subsidence is likely multifactorial, related to component loosening, osteolysis, component malalignment, and avascular necrosis.[32]

Polyethylene Liner Fracture and Displacement

TARs may be fixed- or mobile-bearing, with the fixed-bearing design more susceptible to shear forces at the prosthesis-bone interface given the inherent constraint of the articulation. In mobile-bearing implants, the polyethylene may translate and rotate with respect to the tibia, thus dissipating shear forces that would otherwise be transmitted to the tibia and talus; however, with the added motion between the polyethylene and the tibia, there is less stability at the articulation and therefore a greater risk of polyethylene edge loading and fracture.[9] In the United States, the Scandinavian total ankle replacement (STAR) is the most commonly used mobile-bearing design. The polyethylene component in the STAR includes radiopaque markers that can help to identify liner displacement or fracture
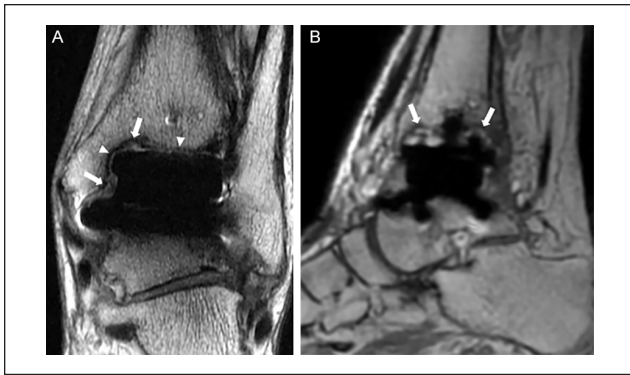
Figure 2. Two patients with tibial component loosening. (A) Coronal intermediate-weighted high-bandwidth FSE image of an Infinity TAR in an 82-year-old man shows near circumferential fibrous membrane (arrowheads) and osseous resorption (arrows) about the tibial component. (B) Sagittal HyperMAVRIC SL image of a Vantage TAR in a 61-year-old woman shows near circumferential osseous resorption (arrows) about the tibial component.

on radiography but, with or without these markers, MRI can demonstrate polyethylene liner location and integrity. Additional factors that may predispose to liner failure include malalignment (resulting in elevated contact pressures) and ligamentous laxity that is not corrected at surgery.[36]

Infection

Infection after TAR can be superficial, involving only the soft tissues, or can be deep, involving the bone or prosthesis. Deep infections are reported to occur in only 1.7% of cases but, of all complications, results in the highest rate of revisions.[18] Because of its ability to evaluate both the soft tissue and bony structures, MRI with metal optimization provides the most comprehensive imaging evaluation for infection. The unparalleled soft tissue contrast of MRI allows for detection of superficial cellulitis, soft tissue abscesses, and tenosynovitis (Figures 5 and 6). When evaluating for soft tissue abscesses, T1 postcontrast images are obtained with high receiver bandwidth to decrease metal artifact. HyperMAVRIC SL sequences allow visualization of the periprosthetic soft tissues to confirm or refute extension of infection to the joint and prosthetic components, while simultaneously evaluating the bone for osteomyelitis.

Heterotopic Ossification

Although commonly seen after TAR, the prevalence of heterotopic ossification (HO) remains unclear, with reports ranging from 3.8% to 98% and disparity in the literature possibly related to differences in HO definition, evaluation

methodology, type of TAR, and follow-up time points.[35] Defining HO as any new osseous formation observed on postoperative radiographs at a minimum of 6 weeks after surgery, Manegold et al[35] found that nearly all patients developed HO after TAR. However, development of HO does not necessarily result in symptoms. Studies suggest that, although HO may be symptomatic in some cases and require operative debridement, the degree of HO present after surgery does not correlate with patients' clinical outcomes, pain, or postoperative range of motion.[8,37]

Gutter Impingement

The etiology of gutter impingement after TAR is multifactorial, with pain localized to the medial or lateral gutter because of osseous or soft tissue impingement. Symptomatic impingement can occur between either the native talar bone or the talar component against the medial or lateral malleolus. This may be due to insufficient talo-malleolar distance.[41] Technical factors such as oversizing of the talar component, especially if preemptive gutter debridement is not performed, may result in an insufficient talo-malleolar distance. On the other hand, if the polyethylene liner is undersized, the talus and its component are recessed further into the mortise, thereby also decreasing the talo-malleolar distance. The talus may also become further recessed into the mortise if talar component subsidence occurs, resulting in an insidious development of gutter impingement. Impingement from malalignment may be secondary to rotational malalignment of the components in the transverse plane, or varus/valgus malalignment that can result from inadequate correction at the time of surgery and made worse with uneven polyethylene wear. With increased osseous resection or component subsidence, the calcaneus may also impinge on the lateral malleolus in valgus malalignment (Figure 7).

Periprosthetic Fracture and Stress Reaction

Periprosthetic fracture is a relatively uncommon complication that may occur either intraoperatively or postoperatively. The incidence of postoperative periprosthetic fractures is 2%, whereas intraoperative fractures can occur in 2.2% to 8.1% of cases.[18] Intraoperative fractures may occur secondary to overexcursion of the oscillating saw, excessive bone resection, and oversizing of the prosthetic component relative to the osteotomy bed. Postoperative fractures may be characterized as either traumatic or stress-induced. Stress fractures tend to occur at the medial malleolus, often related to component malposition, either in varus, because of increased loading of the medial malleolus, or in valgus, because of increased traction on the medial malleolus by the deltoid ligament.[34] Periprosthetic fracture of the tibia is much more common than that of the talus, which has
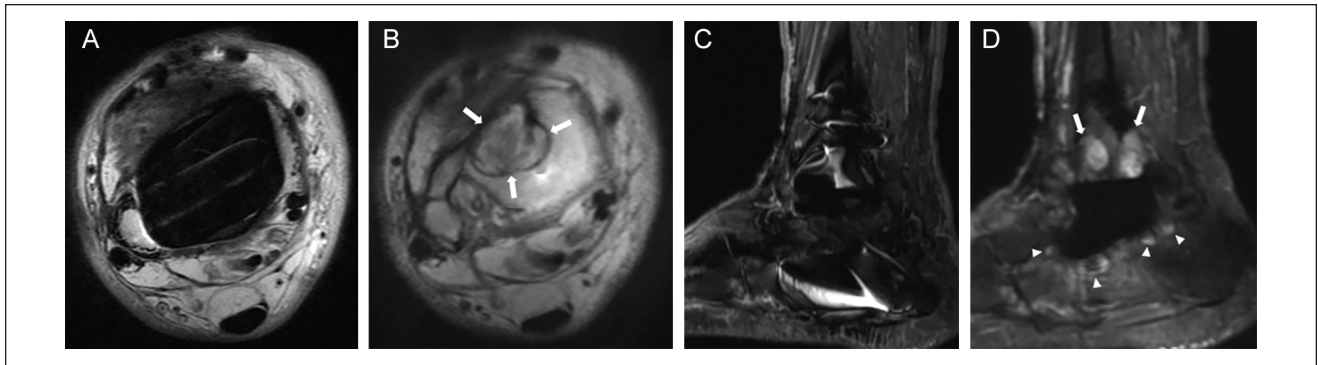
Figure 3. Agility TAR in a 79-year-old man with periprosthetic osteolysis. (A) Axial high-bandwidth intermediate-weighted FSE image just above the tibial component is completely obscured by through-plane distortion while (B) the concurrent axial HyperMAVRIC SL image at the same level reveals prominent osteolysis (arrows) in the distal tibia. (C) Sagittal high-bandwidth STIR image also demonstrates marked image distortion but (D) the STIR MAVRIC SL image in the same plane again clearly demonstrates the tibial osteolysis (arrows) along the bone-metal interface, as well as additional smaller foci of osteolysis in the calcaneus (arrowheads). Of note, the revised stemmed talar component is subsided with abnormal angulation and seated in the calcaneus.
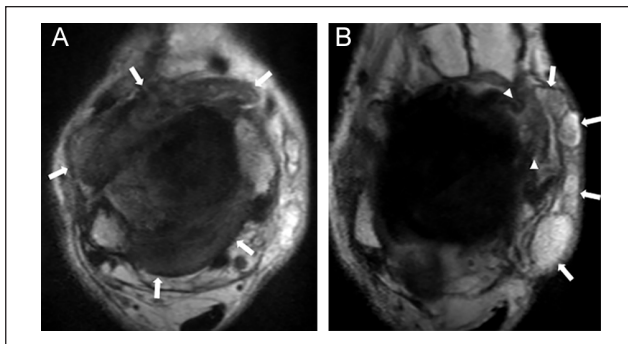
Figure 4. Axial HyperMAVRIC SL images in the same patient as in Figure 3. (A) At the level of the tibial component, dense polymeric synovial debris distends the pseudocapsule both anteriorly and posteriorly (arrows). (B) The fluid decompresses through a dehiscent anteromedial pseudocapsule (arrowheads), forming a heterogeneously hyperintense loculated collection (arrows) dissecting posteriorly in the medial subcutaneous fat, reflecting extracapsular extension of this process.

Figure 5. Infinity TAR in a 59-year-old man with prosthetic joint infection. (A) Sagittal STIR MAVRIC SL image shows a fluid collection (arrowhead) in the anteromedial soft tissues with a sinus tract (arrow) extending to the ventral aspect of the tibial component. (B) Axial high-bandwidth T1 postcontrast image shows a thick rim of enhancement (arrowheads) around the collection as well as an enhancing phlegmonous collection (arrow) more centrally along the anterior aspect of the tibia.

a recently reported incidence rate of 1%, all occurring in implants with a talar stem.[10] Stress reactions without associated fracture line may be seen about either the tibial or the talar component (Figure 8).

Adjacent Joint Degeneration

Compared to ankle arthrodesis, TAR preserves range of motion in the ankle joint, thereby resulting in less stress on the neighboring joints. Gait analysis parameters and range of motion are better after TAR than ankle arthrodesis, but the risk of adjacent (ie, subtalar or talonavicular) joint degeneration after TAR is not eliminated.[13,37] A review by Knecht et al[25] demonstrated a 19% rate of progressive

subtalar arthritis and 15% rate of progressive talonavicular arthritis, with a minimum follow-up of 2 years after Agility TAR.[13] Kerkhoff et al[24] reported development of arthritis in the subtalar and talonavicular joints of 9% and 11%, respectively, with a minimum follow-up of 7.5 years after STAR.[37] The frequency of adjacent joint arthritis following ankle arthrodesis is generally higher, although this could be partially related to longer terms of follow-up for patients with ankle arthrodesis.[37] In addition, reported incidences of adjacent joint arthritis after arthrodesis vary widely (10%-60%), and these studies are limited by the use of radiographs to determine progression of arthritis. MRI would be more useful to evaluate for this complication given its ability to detect subtle cartilage changes in the surrounding joints.
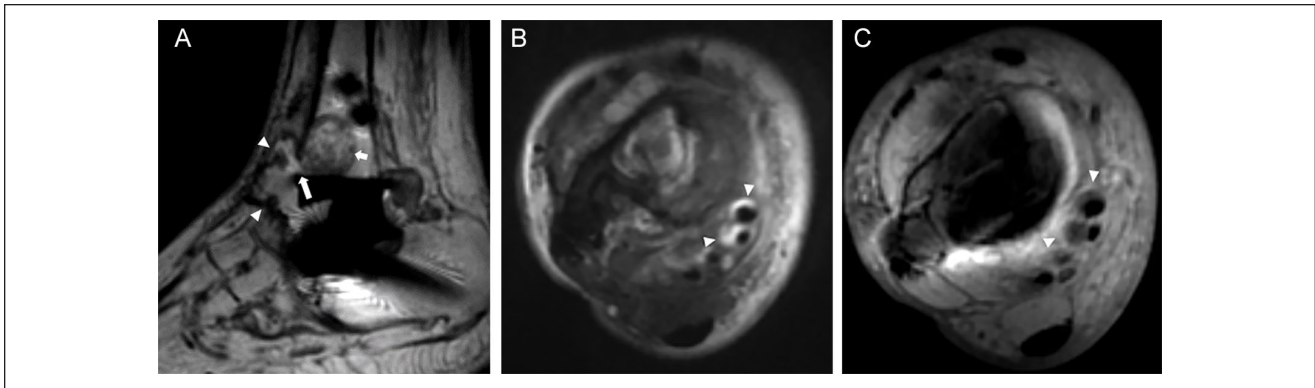
Figure 6. Magnetic resonance imaging of the same patient as in Figures 3 and 4 performed 7 months later demonstrates interval development of a prosthetic joint infection. (A) Sagittal HyperMAVRIC SL image shows prominent synovial expansion (arrowheads) in the anterior joint recess, now in open communication (long arrow) with the region of tibial osteolysis (short arrow), reflecting osteomyelitis. (B) Axial STIR MAVRIC SL image more superiorly shows fluid within the posterior tibial and flexor digitorum longus tendon sheaths (arrowheads), with (C) axial postcontrast T1 imaging demonstrating enhancement of the tendon sheaths (arrowheads) and surrounding soft tissues, reflecting septic tenosynovitis.
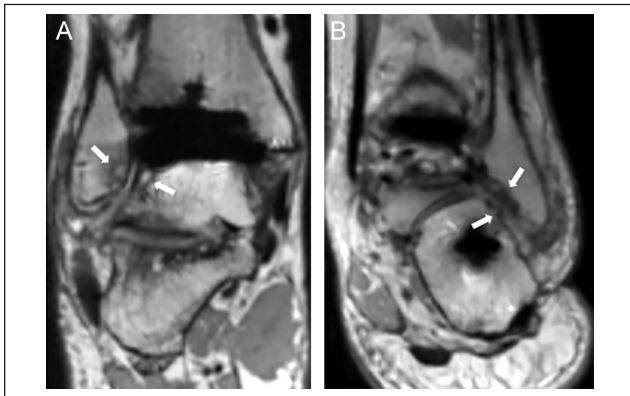
Figure 7. Two patients with lateral gutter impingement. (A) Coronal HyperMAVRIC SL image of a Vantage TAR in a 61-year-old man shows degenerative subchondral cystic changes at the inner margin of the lateral malleolus and the lateral aspect of the talus (arrows). (B) Coronal HyperMAVRIC SL image of a Salto Talaris TAR in a 63-year-old man shows a marked valgus alignment of the hindfoot. The calcaneus is laterally subluxed, with cortical irregularity at the abnormal articulation between the lateral aspect of the calcaneus and the inner margin of the lateral malleolus (arrows).

Conclusion

High-resolution MRI with metal optimization techniques provides a comprehensive imaging assessment of the painful TAR. Although radiography and CT currently have important roles in follow-up and assessment for complications, they are both limited in evaluation of the soft tissues, in addition to the inherent limitations of evaluating a 3-dimensional structure using a 2-dimensional projection in the case of radiography and streak artifact in the case of CT. Ultrasonography can provide some soft tissue assessment but is primarily used to guide aspiration because of limited tissue penetration and inability
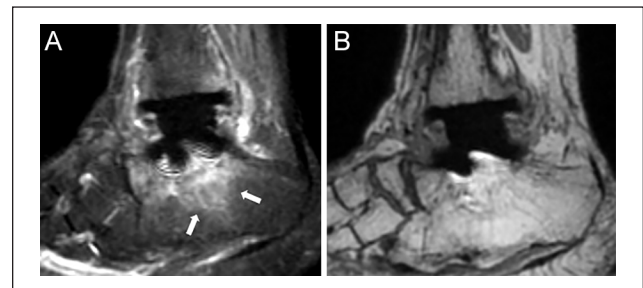
Figure 8. Vantage TAR in a 55-year-old woman in the setting of subtalar and calcaneocuboid arthrodesis. (A) Sagittal STIR MAVRIC SL image demonstrates prominent bone marrow edema (arrows) subjacent to the talar component, without a corresponding fracture line on the sagittal HyperMAVRIC SL sequence (B), reflecting stress reaction.

to assess the bony structures. One of the most common clinical dilemmas after TAR is the painful arthroplasty with normal radiographs/CT and it is in this setting that MRI with dedicated HyperMAVRIC SL imaging is the most useful. Using these new and emerging techniques, MRI can assess the integrity of the soft tissue structures as well as detect subtle periprosthetic bony abnormalities, enabling early diagnosis and potentially better treatment options for patients.

Ethical Approval

Ethical approval for this study was obtained from the Institutional Review Board (ID 2021-0332).

Declaration of Conflicting Interests

The author(s) declared no potential conflicts of interest with respect to the research, authorship, and/or publication of this article. There are several disclosures on the ICJME forms involving 3 of the authors.

ORCID iD

Ji Lin, MD, https://orcid.org/0000-0001-9062-0868

References

1. Adams SB. Salvage arthrodesis for failed total ankle replacement. *Foot Ankle Clin*. 2020;25(2):281-291.
2. Archibeck MJ, Jacobs JJ, Roebuck KA, et al. The basic science of periprosthetic osteolysis. *Instr Course Lect*. 2001;50:185-195.
3. Athanasou NA. The pathobiology and pathology of aseptic implant failure. *Bone Joint Res*. 2016;5(5):162-1628.
4. Atkins GJ, Haynes DR, Howie DW, Findlay DM. Role of polyethylene particles in peri-prosthetic osteolysis: a review. *World J Orthop*. 2011;2(10):93-101.
5. Bartel AFP, Roukis TS. Total ankle replacement survival rates based on Kaplan-Meier survival analysis of national joint registry data. *Clin Podiatr Med Surg*. 2015;32:483-494.
6. Bonnin M, Gaudot F, Laurent JR, Ellis S, Colombier JA, Judet T. The Salto total ankle arthroplasty: survivorship and analysis of failures at 7 to 11 years. *Clin Orthop Rel Res*. 2011;469(1):225-236.
7. Brulefert K, Cordova LA, Brulin B, et al. Pro-osteoclastic in vitro effect of polyethylene-like nanoparticles: involvement in the pathogenesis of implant aseptic loosening. *J Biomed Mater Res A*. 2016;104(11):2649-2657.
8. Choi WJ, Lee JW. Heterotopic ossification after total ankle arthroplasty. *J Bone Joint Surg Br*. 2011;93:1508-1512.
9. Conti SF, Wong YS. Complications of total ankle replacement. *Clin Orthop Relat Res*. 2001;391:105-114.
10. Day J, Kim J, Ellis SJ, et al. Periprosthetic fracture of the talus following total ankle replacement: a case series. *Foot Ankle Orthop*. 2020;5(4). https://doi.org/10.1177%2F2473011420S00186
11. Del Grande F, Santini F, Herzka DA, et al. Fat-suppression techniques for 3-T MR imaging of the musculoskeletal system. *Radiographics*. 2014;34(1):217-233.
12. Dillenseger JP, Molière S, Choquet P, et al. An illustrative review to understand and manage metal-induced artifacts in musculoskeletal MRI: a primer and updates. *Skeletal Radiol*. 2016;45(5):677-688.
13. Easley ME, Adams SB, Hembree WC, et al. Results of total ankle arthroplasty. *J Bone Joint Surg Am*. 2011;93(15):1455-1468.
14. Espinosa N, Klammer G, Wirth SH. Osteolysis in total ankle replacement: how does it work? *Foot Ankle Clin*. 2017;22:267-275.
15. Fritz J, Lurie B, Miller TT, et al. MR imaging of hip arthroplasty implants. *Radiographics*. 2014;34(4):106-133.
16. Fritz J, Lurie B, Potter HG. MR imaging of knee arthroplasty implants. *Radiographics*. 2015;35(5):1483-1501.
17. Gaden MT, Ollivere BJ. Periprosthetic aseptic osteolysis in total ankle replacement: cause and management. *Clin Podiatr Med Surg*. 2013;30(2):145-155.
18. Glazebrook MA, Arsenault K, Dunbar M. Evidence-based classification of complications in total ankle arthroplasty. *Foot Ankle Int*. 2009;30(10):945-949.
19. Gurbani A, Demetracopoulos C, O'Malley M, et al. Correlation of single-photon emission computed tomography results with clinical and intraoperative findings in painful total ankle replacement. *Foot Ankle Int*. 2020;41(6):639-646.
20. Hutchinson B, Schweitzer MJ. Revision surgery for failed total ankle replacement. *Clin Podiatr Med Surg*. 2020;37(3):489-504.
21. Jeyaseelan L, Park SS-H, Al-Rumaih H, et al. Outcomes following total ankle arthroplasty: a review of the registry data and current literature. *Orthop Clin North Am*. 2019;50:539-548.
22. Jonitz-Heincke A, Lochner K, Schulze C, et al. Contribution of human osteoblasts and macrophages to bone matrix degradation and proinflammatory cytokine release after exposure to abrasive endoprosthetic wear particles. *Mol Med Rep*. 2016;14(2):1491-1500.
23. Kaushik SS, Marszalkowski C, Koch KM. External calibration of the spectral coverage for three-dimensional multispectral MRI. *Magn Reson Med*. 2016;76(5):1494-1503.
24. Kerkhoff YRA, Kosse NM, Metsaars WP, et al. Long-term functional and radiographic outcome of a mobile bearing ankle prosthesis. *Foot Ankle Int*. 2016;37(12):1292-1302.
25. Knecht SI, Estin M, Callaghan JJ, et al. The Agility total ankle arthroplasty. Seven to sixteen-year follow-up. *J Bone Joint Surg Am*. 2004;86(6):1161-1171.
26. Kobayashi A, Minoda Y, Kadoya Y, et al. Ankle arthroplasties generate wear particles similar to knee arthroplasties. *Clin Orthop Relat Res*. 2004;424:69-72.
27. Koch KM, Brau AC, Chen W, et al. Imaging near metal with a MAVRIC-SEMAC hybrid. *Magn Reson Med*. 2011;65(1):71-82.
28. Koch KM, Hargreaves BA, Pauly KB, Chen W, Gold GE, King KF. Magnetic resonance imaging near metal implants. *J Magn Reson Imaging*. 2010;32(4):773-787.
29. Labek G, Klaus H, Schlichtherle R, et al. Revision rates after total ankle arthroplasty in sample-based clinical studies and national registries. *Foot Ankle Int*. 2011;32(8):740-745.
30. Labek G, Thaler M, Janada W, et al. Revision rates after total joint replacement: cumulative results from worldwide register dataset. *J Bone Joint Surg Br*. 2011;93(3):293-297.
31. Labek G, Todorov S, Iovanescu L, Stoica CI, Bohler N. Outcome after total ankle arthroplasty—results and findings from world-wide arthroplasty registers. *Int Orthop*. 2013;37(9):1677-1682.
32. Li S-Y, Myerson MS. Management of talar component subsidence. *Foot Ankle Clin*. 2017;22:361-389.
33. Lui TH, Roukis TS. Arthroscopic management of complications following total ankle replacement. *Clin Podiatr Med Surg*. 2015;32(4):495-508.
34. Manegold S, Haas NP, Tsitsilonis S, et al. Periprosthetic fractures in total ankle replacement: classification system and treatment algorithm. *J Bone Joint Surg Am*. 2013;95(9):815-820.
35. Manegold S, Springer A, Landvoigt A, et al. Heterotopic ossification after total ankle replacement: the role of prosthesis alignment. *Eur Foot Ankle Soc*. 2017;23:122-127.

36. Mulcahy H, Chew FS. Current concepts in total ankle replacement for radiologists: complications. *AJR Am J Roentgenol*. 2015;205:1244-1250.

37. Omar IM, Abboud SF, Youngner JM. Imaging of total ankle arthroplasty: normal imaging findings and hardware complications. *Semin Musculoskelet Radiol*. 2019;23(2):177-194.

38. Purdue PE, Koulouvaris P, Potter HG, et al. The cellular and molecular biology of periprosthetic osteolysis. *Clin Orthop Relat Res*. 2007;454(454):251-261.

39. Sadoghi P, Liebensteiner M, Agreiter M, Leithner A, Bohler N, Labek G. Revision surgery after total joint arthroplasty: a complication-based analysis using worldwide arthroplasty registers. *J Arthroplasty*. 2013;28(8):1329-1332.

40. Schipper ON, Haddad SL, Pytel P, Zhou Y. Histological analysis of early osteolysis in total ankle arthroplasty. *Foot Ankle Int*. 2017;38(4):351-359.

41. Schuberth JM, Wood DA, Christensen JC. Gutter impingement in total ankle arthroplasty. *Foot Ankle Spec*. 2016;9(2):145-158.

42. Sofka CM. Postoperative magnetic resonance imaging of the foot and ankle. *J Magn Reson Imaging*. 2013;37(3):556-565.

43. Spirit A, Assal M, Hansen ST. Complications and failure after total ankle arthroplasty. *J Bone Joint Surg Am*. 2004;86(6):1172-1178.

44. Sundfeldt M, Widmark M, Johansson CB, et al. Effect of submicron polyethylene particles on an osseointegrated implant: an experimental study with a rabbit patella-femoral prosthesis. *Acta Orthop Scand*. 2002;73(4):416-424.

45. Zochowski KC, Miranda MA, Cheung J, et al. MRI of hip arthroplasties: comparison of isotropic Multiacquisition Variable-Resonance Image Combination Selective (MAVRIC SL) acquisitions with a conventional MAVRIC SL acquisition. *AJR Am J Roentgenol*. 2019;213(6):W277-W286.